Letter | Editors' Suggestion

Nonlocal conductance spectroscopy of Andreev bound states in gate-defined InAs/Al nanowires

Andreas Pöschl,[1] Alisa Danilenko,[1] Deividas Sabonis,[1,2] Kaur Kristjuhan,[1] Tyler Lindemann,[3] Candice Thomas,[3] Michael J. Manfra,[3,4] and Charles M. Marcus[1,*]

[1]*Center for Quantum Devices, Niels Bohr Institute, University of Copenhagen, 2100 Copenhagen, Denmark*
[2]*Laboratory for Solid State Physics, ETH Zürich, CH-8093 Zürich, Switzerland*
[3]*Department of Physics and Astronomy, and Birck Nanotechnology Center, Purdue University, West Lafayette, Indiana 47907, USA*
[4]*School of Materials Engineering, and School of Electrical and Computer Engineering, Purdue University, West Lafayette, Indiana 47907, USA*

(Received 6 April 2022; accepted 14 November 2022; published 12 December 2022)

The charge character of Andreev bound states (ABSs) in a three-terminal semiconductor-superconductor hybrid nanowire was measured using local and nonlocal tunneling spectroscopy. The device is fabricated using an epitaxial InAs/Al two-dimensional heterostructure with several gate-defined side probes. ABSs give rise to distinct local and nonlocal conductance signatures which evolve as a function of magnetic field and gate voltage. At high magnetic fields, ABSs are found to oscillate around zero as a function of gate voltage, with modifications of their charge consistent with expectations for the total Bardeen-Cooper-Schrieffer charge of ABSs.

DOI: 10.1103/PhysRevB.106.L241301

In semiconducting nanowires (NWs) proximitized by a layer of superconductor, tunneling spectroscopy from a normal-metal contact reveals a spectrum of particle-hole symmetric Andreev bound states (ABSs) localized within the device, confined either by electrostatic gates, device boundaries, or defects [1]. The process of Andreev reflection enables a measurable current in the presence of states below the superconducting gap. This reflection of electrons and holes at the boundary between normal and superconducting phase bears similarity with the reflection of photons from a phase-conjugating mirror [2–4]. Recently, a device geometry has been realized that makes it possible to measure tunneling currents at two normal leads connected to the same proximitized NW while keeping the parent superconductor grounded [5,6].

Nonlocal conductance is measured as a differential current response on one probe in response to a differential voltage applied on another probe. For applied voltages smaller than the superconducting gap, nonlocal transport is mediated by Andreev states that couple to the relevant tunnel probes. Theoretical studies predict a characteristic signature in nonlocal conductance of a topological phase transition in NWs with particular spin-orbit and Zeeman effect [7–10]. Characteristic symmetry relations relating local and nonlocal conductances have been reported experimentally [5]. The closing of the induced gap measured in nonlocal conductance in an applied field has also been reported experimentally [6]. Using the same transport processes, quantum dots coupled to one superconducting and two normal leads have been used to demonstrate Cooper-pair splitting [11–14]. Nonlocal spectroscopy of subgap states induced by quantum dot states has been reported in vapor-liquid-solid grown NWs and carbon nanotubes [13,15,16].

Here, we investigate and compare local and nonlocal conductance measurements on a gate-defined NW formed from an InAs two-dimensional electron gas (2DEG) with epitaxial Al. By using a patterned 2DEG, lithographically defined gate-controlled tunneling probes can be coupled laterally to the NW rather than at the ends, allowing several equivalent probes along the side of the NW. We observed characteristic local and nonlocal signatures of ABSs that have been intentionally tuned to couple neighboring probes. Three similar

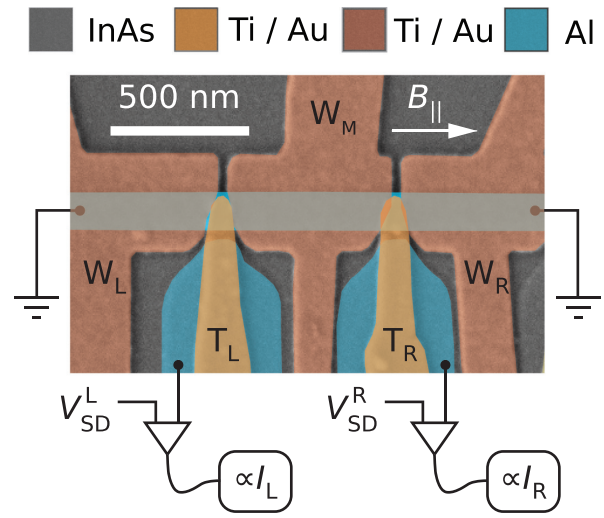

FIG. 1. False-color electron micrograph of device 1. A proximitized quasi-one-dimensional NW is formed in the InAs quantum well (gray) under the strip of superconducting Al (blue) by lateral electrostatic confinement from the gates W_L, W_M, W_R (red). Probes made from Al are separated by a tunnel barrier from the NW and allow for measurements of the tunneling currents I_L, I_R into the NW. The gates T_L and T_R (orange) tune the tunnel barriers between the NW and the probes.

*marcus@nbi.ku.dk

multiprobe devices were measured. Device 1 had superconducting leads that were driven normal by a magnetic field applied along the NW; device 2 had the epitaxial superconductor in the leads removed. Except for supercurrent signatures in local (but not nonlocal) conductance at low fields (below 0.2 T) due to superconductivity in the leads, devices 1 and 2 showed similar behavior. A third measured device was operational but did not show clear, extended ABSs between adjacent probes. Micrographs and data from device 2 and device 3 are shown in the Supplemental Material (SM) [17].

A micrograph of device 1 is shown in Fig. 1. The device consists of a superconducting strip of Al, defined by wet etching of the epitaxial Al, on top of a shallow 2DEG formed in an InAs quantum well. The strip serves both to induce superconductivity in the InAs by proximity and to define the wire width by screening the surrounding gates. Two superconducting probes patterned in the same lithographic step were defined 50 nm away from the superconducting strip, leaving a narrow gap of exposed semiconductor between the NW and the probe. Ti/Au gates insulated by HfO_x gate dielectric were used to control the probe conductance and the electrostatic environment around the NW. Gates labeled W_L, W_M, and W_R cover different segments of the Al strip and electrostatically confine an approximately 100-nm-wide NW. Gates T_L and T_R deplete the semiconductor between NW and the respective left and right probes, controlling the tunnel barrier. The ends of the superconducting strip were connected to ground planes of superconducting Al.

Separate current-to-voltage converters on two tunnel probes allow simultaneous measurement of currents I_L and I_R as a function of source-drain bias voltages V_{SD}^L and V_{SD}^R (positive current is defined as flowing from the amplifier to the device). Lock-in detection following Ref. [5] was used to measure the local and nonlocal differential tunneling conductances

$$G_{LL} = dI_L/dV_{SD}^L, \quad G_{LR} = dI_L/dV_{SD}^R, \tag{1}$$

and G_{RR}, G_{RL} defined analogously. Further details are given in the SM [17] (see, also, Ref. [S1] therein).

To confine an ABS in a segment of NW, a modulation of the potential along the NW was created using gates W_L, W_M, W_R. Setting V_{WL} and V_{WR} to −4.50 V created a hard, superconducting gap with no subgap states in these segments. The middle gate voltage V_{WM} was then set to −3.02 V, less negative than its neighboring gates. Local and nonlocal conductances Eq. (1) as a function of magnetic field along the NW, $B_{||}$, are shown in Fig. 2. Above $B_{||} > 0.2$ T, the gap of the Al probes turns soft, providing gapless tunnel probes [18]. Both local tunneling conductances G_{LL} and G_{RR} show subgap resonances that emerge at low magnetic fields from the continuum at high bias and cross zero voltage bias at $B_{||} = 1.6$ T. We associate these resonances with an extended ABS in the 0.6-μm-long NW segment under gate W_M due to the appearance in both local tunneling conductances with identical dependence on magnetic field and gate voltage V_{WM}, discussed below. Hybridization of the ABS with an accidental resonance in one of the tunnel barriers was reported previously [19].

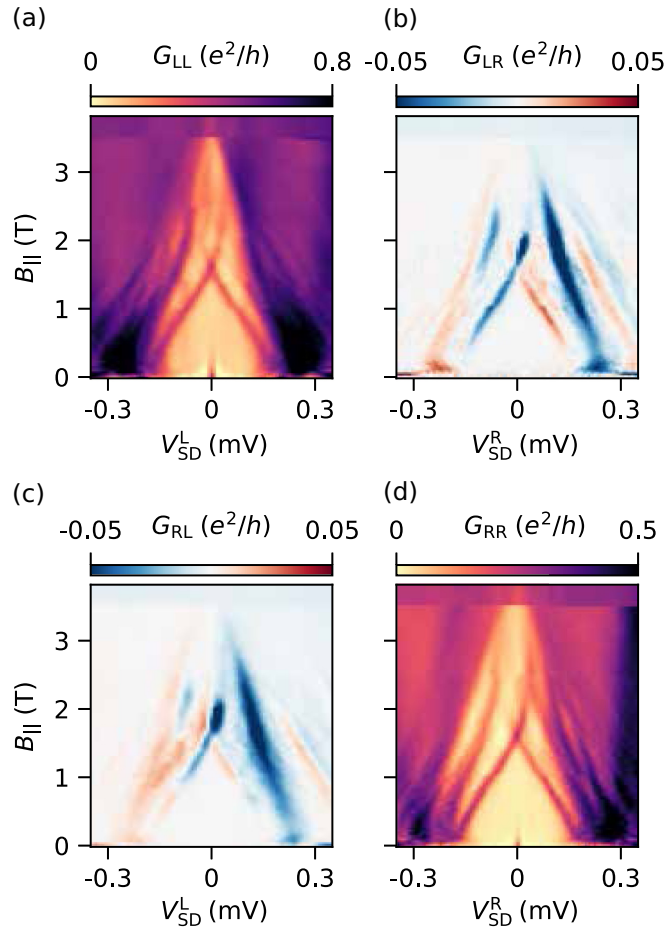

FIG. 2. Local (LL and RR) and nonlocal (LR and RL) differential conductances as a function of magnetic field $B_{||}$ parallel to the NW, at $V_{WM} = -3.02$ V (see extended ranges of V_{WM} in Fig. 3). (a), (d) Local conductances reveal subgap states that cross zero bias. (b), (c) Subgap states also appear in the nonlocal conductances. Note that local differential conductances are positive everywhere, while nonlocal conductances are roughly balanced around zero.

Nonlocal conductances G_{LR} and G_{RL} were of order $5 \times 10^{-2}\, e^2/h$, roughly a factor of 10 smaller than corresponding local conductances. Comparing these values to simulation suggests low-to-moderate disorder [7,9]. Larger nonlocal conductance, $G_{LR}, G_{RL} > 2 \times 10^{-2}\, e^2/h$ at higher bias presumably reflects the field-dependent superconducting gap, $\Delta(B_{||})$, of the Al layer. For magnetic fields below the zero crossing of the ABSs, there is a region of unmeasurably small nonlocal conductance around zero bias, which extends to $V_{SD}^{L/R}$ values marking the ABS energy. The ABSs are the lowest lying excited states that extend over the full segment of NW under gate W_M. Their energy therefore sets the size of the energy gap Δ_{ind} that is induced in the semiconductor by proximity effect and Zeeman energy. Exponentially suppressed nonlocal conductance is expected for $eV_{SD}^{L/R} < \Delta_{ind}$ for NWs that are longer than the wave-function decay length at these energies [7]. In the voltage range $\Delta_{ind} < eV_{SD} \leqslant \Delta$, nonlocal conductance can be interpreted as transport through excited states.

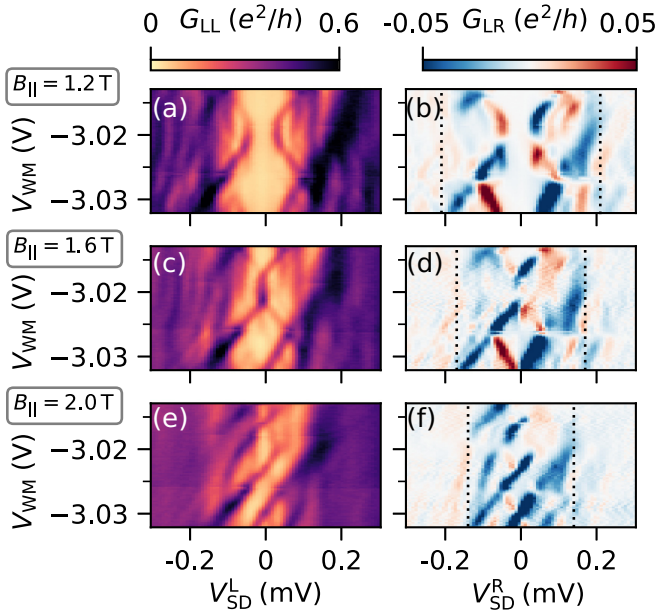

FIG. 3. Local conductance G_{LL} and nonlocal conductance G_{LR} as a function of V_{WM} at three different values of magnetic field $B_{||}$. (a) Subgap states appear as lobes in the superconducting gap. (b) The lowest excited state appears together with a spectrum of higher excited states in the nonlocal conductance. (c) At $B_{||} = 1.6\,\mathrm{T}$ the ABSs merge at zero bias. (d) The nonlocal conductance is suppressed around that region. (e) At $B_{||} = 2\,\mathrm{T}$, the ABSs intersect, forming a low-energy state that oscillates around zero bias. (f) The nonlocal conductance changes sign at the turning points of the low-energy state. The dashed lines in (b), (d), (f) indicate the gap size Δ of the superconducting Al.

Previous studies focused on the gate-voltage dependence of nonlocal conductance in the absence of a magnetic field [5]; here we report the evolution of nonlocal conductance at finite magnetic fields. At a magnetic field of $B_{||} = 1.2\,\mathrm{T}$, the ABSs trace out a pair of lobes that do not reach zero bias as a function of gate voltage V_{WM}, as seen in the the local conductance G_{LL} [see Fig. 3(a)]. The corresponding nonlocal conductance G_{LR}, plotted in Fig. 3(b), is largest at a value V_{SD}^{R} that tracks the position of the low energy subgap state in G_{LL}. Following this state, the nonlocal conductance changes sign in two cases. The first case is a value V_{WM} at which the ABS reaches a minimum in energy. The second case are points where two ABSs cross, which leads to the energy of the lowest lying state changing its slope abruptly from positive to negative and vice versa. Note that there is a spectrum of additional excited states visible at higher bias values V_{SD}^{R}. We interpret these states as a result of the NW being sufficiently long such that the spacing between excited states is decreased [20]. A similarly dense spectrum of excited states has been absent in nonlocal conductance measurements on proximitized quantum dots [15] and shorter NWs [5].

At a magnetic field of $B_{||} = 1.6\,\mathrm{T}$, the lowest ABSs merge at zero voltage bias for a small interval of V_{WM}, as seen in local conductance in Fig. 3(c). Within this range, the nonlocal conductance through the ABS is much smaller than for values of V_{WM} where the ABSs are away from zero bias [see Fig. 3(d)]. This can be understood as a result of the rates for quasiparticle transmission and crossed Andreev reflection being equal at this point due to particle-hole symmetry [21,22]. Nonlocal conductance vanishes at the crossing point as it is proportional to the difference of these two rates [22–24]. At a magnetic field $B_{||} = 2\,\mathrm{T}$, the ABSs intersect, creating a low-energy state that oscillates around zero bias, as seen in Fig. 3(e). G_{LL} shows an asymmetry with respect to V_{SD}^{L}. For all magnetic field values, the regions of sizable nonlocal conductance $G_{LR} > 2 \times 10^{-2}\, e^2/h$ are confined to a finite bias window which coincides with the superconducting gap size of the Al film, Δ, shown as dashed lines in Fig. 3. This is the expected signature for nonlocal conductance through ABSs [7] in contrast to, e.g., the Coulomb-staircase of a quantum dot. The underlying gap sizes $\Delta(B_{||} = 1.2\,\mathrm{T}) = 0.21\,\mathrm{mV}$, $\Delta(B_{||} = 1.6\,\mathrm{T}) = 0.17\,\mathrm{mV}$, and $\Delta(B_{||} = 2.0\,\mathrm{T}) = 0.14\,\mathrm{mV}$ were determined from an independent local tunneling spectroscopy measurement (see Fig. S3 in the SM [17]).

For three-terminal devices, a finite asymmetry of the local tunneling conductances G_{LL} and G_{RR} with respect to zero source-drain voltage bias is expected. In a linear transport theory, the components of the local and nonlocal conductances which are antisymmetric with respect to source-drain bias are related to each other, namely, the antisymmetric component of the nonlocal conductances $G_{LR}^{anti}(V_{SD}^{R}) = [G_{LR}(V_{SD}^{R}) - G_{LR}(-V_{SD}^{R})]/2$ fulfills the relation

$$G_{LR}^{anti}\left(V_{SD}^{R}\right) = -G_{LL}^{anti}\left(V_{SD}^{L}\right) \tag{2}$$

at subgap voltages $eV_{SD} < \Delta$ as a consequence of particle-hole symmetry and current conservation [5,8]. Analogously, one expects $G_{RL}^{anti}(V_{SD}^{L}) = -G_{RR}^{anti}(V_{SD}^{R})$. We find that these relations are quantitatively fulfilled for the lowest excited state, while they are violated for higher excited states. Consequently, the sum over all local and nonlocal conductances $G_{sum} = G_{LL} + G_{RR} + G_{LR} + G_{RL}$ is symmetric up to source-drain bias voltages of the lowest energy state. This also holds true around crossing points of ABSs, as previously remarked in Ref. [5]. A detailed analysis can be found in the SM [17].

Possible reasons for deviations from the symmetry relations were given in Ref. [5]. More recent experimental results furthermore indicated that nonequilibrium transport may affect nonlocal conductance in particular at source-drain bias above the lowest excited state [25]. In addition, numerical studies have shown that an energy dependence of the tunnel barriers in a nonlinear transport theory can give rise to violations of the symmetry relations [26]. Our results indicate that linear transport theory [7,8,27] adequately describes nonlocal transport up to energies of the lowest excited state.

The quantity

$$Q_R = \mathrm{sign}\left(V_{SD}^{R}\right) \frac{G_{LR}^{sym}\left(V_{SD}^{R}\right)}{G_{LR}^{anti}\left(V_{SD}^{R}\right)}\bigg|_{E=eV_{SD}^{R}} \tag{3}$$

of a subgap state at energy $E = eV_{SD}^{R}$ can be extracted from the antisymmetric and symmetric components of the measured nonlocal conductance $G_{LR}(V_{SD}^{R})$ [5]. An equivalent quantity Q_L can be defined based on $G_{RL}(V_{SD}^{L})$. The symmetric and antisymmetric components of the nonlocal conductance G_{LR} measured at a magnetic field value $B_{||} = 2\,\mathrm{T}$ are plotted as a function of source-drain voltage in Figs. 4(a) and 4(b). The values stemming from the low-energy state were extracted

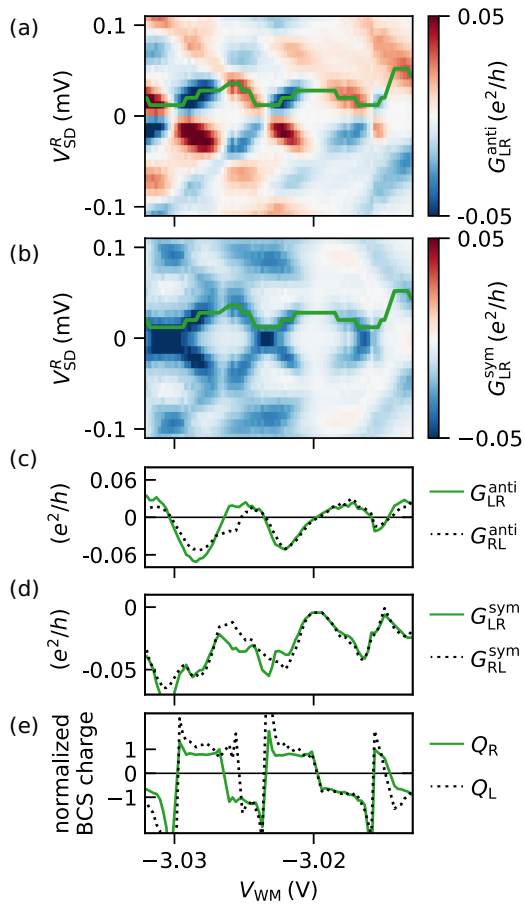

FIG. 4. (a), (b) antisymmetric and symmetric component of the nonlocal conductance G_{LR} measured at $B_{||} = 2$ T. (c), (d) Antisymmetric and symmetric part of the nonlocal conductances G_{LR}, G_{RL} extracted at the position of the lowest lying state marked by the green lines in (a), (b). (e) Resulting values for Q_L and Q_R are approximately equal and show clear oscillations between $+1$ and -1. Positive (negative) values of Q_j coincide with regions of positive (negative) slope of the state energy as a function of V_{WM}.

along the positions given by the green lines in Figs. 4(a) and 4(b).

Extracted antisymmetric and symmetric parts of G_{LR} (solid green) and G_{RL} (dotted black) are shown in Figs. 4(c) and 4(d). These values correspond to the conductances that enter the expressions for Q_R and Q_L. Note that symmetric and antisymmetric parts of G_{LR} and G_{RL} are roughly equal. The resulting values for Q_L and Q_R according to Eq. (3) are shown in Fig. 4(e). Q_L closely follows Q_R.

Bound states in a proximitized semiconductor have both spin and charge degrees of freedom which can show a nontrivial texture along the spatial extent of a bound state. Q_L captures the difference of the squared particle and hole components normalized to the local wave-function weight at the position of the left conductance probe, i.e., the normalized local BCS charge [5,8,27–29]. $Q_L = 1$, for example, corresponds to a completely electronlike state at the location of the left conductance probe. Q_R is defined analogously at the position of the right conductance probe. We find that local charge character on the left and right are approximately equal, $Q_L \approx Q_R$. For device 1 and $B_{||} = 2$ T, there are extended plateaus $Q_j \approx +1$ or $Q_j \approx -1$ ($j \in \{L, R\}$), indicating a state which is locally fully electron or fully holelike. Regions of constant positive Q_j coincide with ranges in V_{WM} where the state energy has a positive slope with respect to V_{WM}. Regions of negative Q_j appear where the state has a negative slope. Abrupt changes in Q_j appear at crossing points of states, both where ABSs cross with their particle-hole conjugate at zero source-drain bias and where different ABSs cross at finite bias. This is in agreement with the interpretation of Q_j measuring the local charge of the bound state. Fully electron and fully holelike ABSs have previously been observed in numerical studies of similar systems due to the inversion of the induced gap by the Zeeman effect [30] and due to multiple noninteracting bands [31]. For lower magnetic field values, at which the ABSs appear as parabolic lobes without zero energy crossings, a continuous change of Q_j from -1 to 1 is found at the point of minimal ABS energy in our experiment (see Fig. S7 in SM [17]). For device 2, the same behavior, namely, $Q_L \approx Q_R$, was observed, with either abrupt changes or continuous crossover from positive to negative Q_j.

The total, integrated charge of a bound state at energy E is expected to be proportional to dE/dV_{WM}, according to a model based on a Bogoliubov-de Gennes Hamiltonian [8]. Integrating the total charge over a range of gate voltages should therefore recover the energy of the subgap state as a function of V_{WM}. We numerically integrated the experimentally determined Q_j after rescaling by a lever arm a and taking into account a linear background b and integration constant c, yielding the inferred energy

$$\widetilde{E}_j = a \int Q_j dV_{WM} + bV_{WM} + c. \tag{4}$$

a, b, and c are free parameters. We find that the resulting curves for $\widetilde{E}_L(V_{WM})$ and $\widetilde{E}_R(V_{WM})$ match the energy evolution $E(V_{WM})$ of the low-energy subgap state over an extended range of V_{WM} (see Fig. S8 in SM [17]). This suggests that the experimentally determined Q_j not only reflects the local charge character of the ABS but serves as a measure for the total charge of the bound states. Deviations from this behavior are expected for longer devices where the ABS charge shows spatial variations [8,27].

In summary, we have performed local and nonlocal conductance spectroscopy in a 2DEG-based NW with integrated side probes and multiple confining gates along the NW length, as a function of magnetic field and gate voltage on a middle segment of the NW surrounded by hard-gap regions created by more-negative gate voltages in adjacent regions. The predicted symmetry relations between the antisymmetric components of local and nonlocal conductances are fulfilled for the lowest excited state. In addition, we find a dense spectrum of excited states that give rise to nonlocal conductance. For the lowest excited state, the extracted charge character is the same at both NW ends. This is similar to previous studies [5] despite a longer NW being used here. At high magnetic fields, the charge character Q_L, Q_R of the low-energy state alternates between fully electron and holelike. The oscillations in the charge character are found to be in agreement with the energy evolution $E(V_{WM})$ of the subgap state which suggests that Q_L and Q_R reflect the total charge of the ABS measured.

In the SM, we show additional data measured on device 1, together with data from device 2 and device 3. The SM also contains further details on the materials used, the device fabrication, and the data analysis [17].

We thank Karsten Flensberg, Max Geier, Torsten Karzig, Andrea Maiani, Dmitry Pikulin, Waldemar Svejstrup, and Georg Winkler for valuable discussions concerning theory, and Abhishek Banerjee, Lucas Casparis, Asbjørn Drachmann, Esteban Martinez, Felix Passmann, Daniel Sanchez, Saulius Vaitiekėnas, and Alexander Whiticar for experimental input. We acknowledge support from the Danish National Research Foundation, Microsoft, and a grant (Project No. 43951) from VILLUM FONDEN.

[1] H. Pan and S. Das Sarma, Phys. Rev. Res. **2**, 013377 (2020).
[2] C. W. J. Beenakker, Phys. Rev. B **46**, 12841 (1992).
[3] C. W. J. Beenakker, in *Quantum Mesoscopic Phenomena and Mesoscopic Devices in Microelectronics* (Springer Netherlands, Dordrecht, 2000), pp. 51–60.
[4] C. W. J. Beenakker, J. P. Dahlhaus, M. Wimmer, and A. R. Akhmerov, Phys. Rev. B **83**, 085413 (2011).
[5] G. C. Ménard, G. L. R. Anselmetti, E. A. Martinez, D. Puglia, F. K. Malinowski, J. S. Lee, S. Choi, M. Pendharkar, C. J. Palmstrøm, K. Flensberg, C. M. Marcus, L. Casparis, and A. P. Higginbotham, Phys. Rev. Lett. **124**, 036802 (2020).
[6] D. Puglia, E. A. Martinez, G. C. Ménard, A. Pöschl, S. Gronin, G. C. Gardner, R. Kallaher, M. J. Manfra, C. M. Marcus, A. P. Higginbotham, and L. Casparis, Phys. Rev. B **103**, 235201 (2021).
[7] T. Ö. Rosdahl, A. Vuik, M. Kjaergaard, and A. R. Akhmerov, Phys. Rev. B **97**, 045421 (2018).
[8] J. Danon, A. B. Hellenes, E. B. Hansen, L. Casparis, A. P. Higginbotham, and K. Flensberg, Phys. Rev. Lett. **124**, 036801 (2020).
[9] H. Pan, J. D. Sau, and S. Das Sarma, Phys. Rev. B **103**, 014513 (2021).
[10] R. Hess, H. F. Legg, D. Loss, and J. Klinovaja, Phys. Rev. B **104**, 075405 (2021).
[11] L. Hofstetter, S. Csonka, A. Baumgartner, G. Fülöp, S. d'Hollosy, J. Nygård, and C. Schönenberger, Phys. Rev. Lett. **107**, 136801 (2011).
[12] L. Hofstetter, S. Csonka, J. Nygård, and C. Schönenberger, Nature (London) **461**, 960 (2009).
[13] Z. Scherübl, G. Fülöp, J. Gramich, A. Pályi, C. Schönenberger, J. Nygård, and S. Csonka, Phys. Rev. Res. **4**, 023143 (2022).
[14] J. Schindele, A. Baumgartner, and C. Schönenberger, Phys. Rev. Lett. **109**, 157002 (2012).
[15] J. Gramich, A. Baumgartner, and C. Schönenberger, Phys. Rev. B **96**, 195418 (2017).
[16] J. Schindele, A. Baumgartner, R. Maurand, M. Weiss, and C. Schönenberger, Phys. Rev. B **89**, 045422 (2014).
[17] See Supplemental Material at http://link.aps.org/supplemental/10.1103/PhysRevB.106.L241301 for information on data analysis, device fabrication, and additional data.
[18] H. J. Suominen, M. Kjaergaard, A. R. Hamilton, J. Shabani, C. J. Palmstrøm, C. M. Marcus, and F. Nichele, Phys. Rev. Lett. **119**, 176805 (2017).
[19] A. Pöschl, A. Danilenko, D. Sabonis, K. Kristjuhan, T. Lindemann, C. Thomas, M. J. Manfra, and C. M. Marcus, Phys. Rev. B **106**, L161301 (2022).
[20] R. V. Mishmash, D. Aasen, A. P. Higginbotham, and J. Alicea, Phys. Rev. B **93**, 245404 (2016).
[21] A. R. Akhmerov, J. P. Dahlhaus, F. Hassler, M. Wimmer, and C. W. J. Beenakker, Phys. Rev. Lett. **106**, 057001 (2011).
[22] A. M. Lobos and S. D. Sarma, New J. Phys. **17**, 065010 (2015).
[23] Y. Takane and H. Ebisawa, J. Phys. Soc. Jpn. **61**, 1685 (1992).
[24] M. P. Anantram and S. Datta, Phys. Rev. B **53**, 16390 (1996).
[25] G. Wang, T. Dvir, N. van Loo, G. P. Mazur, S. Gazibegovic, G. Badawy, E. P. A. M. Bakkers, L. P. Kouwenhoven, and G. de Lange, Phys. Rev. B **106**, 064503 (2022).
[26] A. Melo, C.-X. Liu, P. Rożek, T. Ö. Rosdahl, and M. Wimmer, SciPost Phys. **10**, 037 (2021).
[27] A. B. Hellenes, Local and nonlocal differential conductance spectroscopy of Andreev bound states in three-terminal superconducting devices, Master's thesis, University of Copenhagen, 2019.
[28] D. Sticlet, C. Bena, and P. Simon, Phys. Rev. Lett. **108**, 096802 (2012).
[29] P. Marra and A. Nigro, J. Phys.: Condens. Matter **34**, 124001 (2022).
[30] P. Marra and M. Nitta, Phys. Rev. B **100**, 220502(R) (2019).
[31] B. D. Woods, J. Chen, S. M. Frolov, and T. D. Stanescu, Phys. Rev. B **100**, 125407 (2019).